Geochemistry Geophysics Geosystems G3
AN ELECTRONIC JOURNAL OF THE EARTH SCIENCES
Published by AGU and the Geochemical Society

Article
Volume 8, Number 1
XX Month 2007
XXXXXX, doi:10.1029/2006GC001511
ISSN: 1525-2027

Effective elastic thickness of South America and its implications for intracontinental deformation

M. Pérez-Gussinyé
Institute of Earth Sciences "Jaume Almera," CSIC, Lluis Sole i Sabaris s/n, Barcelona E-08028, Spain (mperez@ija.csic.es)

A. R. Lowry
Department of Geology, Utah State University, 4505 Old Main Hill, Logan, Utah 84322, USA

A. B. Watts
Department of Earth Sciences, University of Oxford, Oxford OX1 3PR, UK

[1] The flexural rigidity or effective elastic thickness of the lithosphere, T_e, primarily depends on its thermal gradient and composition. Consequently, maps of the lateral variability of T_e in continents reflect their lithospheric structure. We present here a new T_e map of South America generated using a compilation of satellite-derived (GRACE and CHAMP missions) and terrestrial gravity data (including EGM96 and SAGP), and a multitaper Bouguer coherence technique. Our T_e maps correlate remarkably well with other proxies for lithospheric structure: areas with high T_e have, in general, high lithospheric mantle shear wave velocity and low heat flow and vice versa. In this paper we focus on the T_e of the stable platform. We find that old cratonic nuclei (mainly Archean and Early/Middle Proterozoic) have, in general, high T_e (>70 km), while the younger Patagonian Phanerozoic terrane has much lower T_e (20–30 km), suggesting that T_e is related to terrane age as has already been noted in Europe. Within cratonic South America, T_e variations are observed at regional scale: relatively lower T_e occurs at sites that have been repeatedly reactivated throughout geological history as major sutures, rift zones, and sites of hot spot magmatism. Today, these low T_e areas are surrounded by large cratonic nuclei. They concentrate most of the intracontinental seismicity and exhibit relatively high surface heat flow and low seismic velocity at 100 km depth. This implies that intracontinental deformation focuses within relatively thin, hot, and hence weak lithosphere, that cratonic interiors are strong enough to inhibit tectonism, and that the differences in lithospheric rigidity, structure, and composition between stable cratons and sites of intracontinental deformation are not transient, and may have been maintained, in some cases, for at least 500 m.y.

Components: 13,516 words, 8 figures.

Keywords: elastic thickness; South America; lithospheric structure; stable platform; intracontinental deformation; satellite and terrestrial gravity.

Index Terms: 1219 Geodesy and Gravity: Gravity anomalies and Earth structure (0920, 7205, 7240); 9360 Geographic Location: South America; 1236 Geodesy and Gravity: Rheology of the lithosphere and mantle (7218, 8160).

Received 14 October 2006; **Revised** 22 January 2007; **Accepted** 12 February 2007; **Published** XX Month 2007.

Pérez-Gussinyé, M., A. R. Lowry, and A. B. Watts (2007), Effective elastic thickness of South America and its implications for intracontinental deformation, *Geochem. Geophys. Geosyst.*, *8*, XXXXXX, doi:10.1029/2006GC001511.

1. Introduction

[2] Continents form by the amalgamation of terranes that have stabilized at different times during Earth's history. In general, old terranes (>1.8 Ga) have a lithosphere that is thicker, more depleted in basaltic constituents and, consequently, more dehydrated than younger ones [*Jordan*, 1978; *O'Reilly et al.*, 2001; *Hirth and Kohlstedt*, 1996]. The combination of these factors is thought to make continental cratonic interiors more resistant to subsequent deformation [e.g., *Pollack*, 1986; *Hirth and Kohlstedt*, 1996].

[3] A measure of the resistance to vertical deformation of the lithosphere is its flexural rigidity or, equivalently, its effective elastic thickness, T_e. A recent map of T_e in Europe, for example, shows that in this continent areas of high T_e are located within older terranes (>1.5 Gyr) where the lithospheric thickness, as inferred from shear wave-velocities and thermal gradient, is much greater than in the younger terranes [*Pérez-Gussinyé and Watts*, 2005]. Since large T_e correlates well with areas where the seismic and thermal lithosphere is thick and vice versa, T_e maps of continents may be used not only to better understand their mechanical properties, but also to image the lateral variability in their structure.

[4] Earth structure is commonly imaged using seismic velocities as a proxy for rock temperature and composition. On the other hand, sensitivity analysis of T_e, indicates that it primarily depends on crustal thickness (a compositional feature) and parameters of power law creep, i.e., temperature, composition and to a lesser degree strain rate [*Lowry and Smith*, 1995; *Burov and Diament*, 1995; *Lowry et al.*, 2000; *Brown and Phillips*, 2000]. Thus T_e mainly depends on temperature and composition and could be used, in principal, to map lithospheric structure in an analogous way as seismic velocities are used. However, while seismic tomography can provide an image of the subsurface at different depths, T_e represents a depth integral of physical properties over the lithosphere. Despite this, T_e affords a view of the lithosphere that complements tomography because it more directly reflects the rheological strength than does seismic velocity. Moreover, mapping lithospheric structure at continent-wide scale using flexural rigidity has become much simpler because of the recent availability of relatively high resolution (1 degree) global grids of satellite-derived free-air gravity data (from GRACE and CHAMP) that can be combined with terrestrial data.

[5] Traditionally, T_e is estimated using either forward (space-domain based) or inverse (spectral-domain based) methods, both of which use topography and gravity anomalies as input data [*Watts*, 2001]. Exact comparison of the results obtained from different regional T_e studies is not necessarily straightforward, however, as T_e estimates are sensitive to the dimensions of the data window, the power spectral estimator and the loading model used.

[6] Loading models include those that assume only surface loads such as the thrust sheets in orogenic belts, and those that consider both surface and subsurface loads, as for example intracrustal thrusts and magmatic underplating. Models that only include surface loads were used during the late 70s and early 80s. While these studies yielded reasonable results for oceanic lithosphere [*Watts et al.*, 1980], they produced very low estimates for cratonic continental lithosphere (e.g., 5–10 km for the cratonic United States [*Banks et al.*, 1977]). *Forsyth* [1985], however, noted that if subsurface loads contribute some fraction to lithospheric loading, T_e would be underestimated by considering surface loading alone. Taking into account surface and subsurface loading, *Forsyth* [1985] and a number of subsequent studies recovered very large T_e (>60 km) values for cratonic interiors.

[7] More recently, *McKenzie* [2003] suggested that long-term erosion and sedimentation over cratons might generate internal loads with no topographic expression. These loads would constitute noise within the flexural model framework, as they would represent density anomalies with no apparent flexural response. *McKenzie* [2003] argued that this potential noise field would bias the spectral methods results using the coherence function and the Bouguer anomaly (Bouguer coherence) but not those obtained from the admittance function and the free-air gravity (free-air admittance). Using the free-air admittance he obtained T_e estimates in cratons that were <25 km. However, subsequently, it has been shown that if the free-air admittance is formulated consistently with the Bouguer coherence, both methods yield similar results (within uncertainties) when applied to synthetic as well as real data (see *Pérez-Gussinyé et al.* [2004] and *Pérez-Gussinyé and Watts* [2005] for a detailed discussion). In Europe, for example, both techniques yield low T_e in young Phanerozoic terranes and large estimates in cratons (T_e > 60 km), where

the topography is subdued and long-term erosion and sedimentation have occurred. This suggests that subsurface loads without topographic expression may not occur [*Pérez-Gussinyé and Watts*, 2005]. Consequently, most spectral methods for T_e estimation use the Bouguer coherence function and a loading model that includes surface and subsurface loading, as is done here.

[8] That T_e may depend on the dimensions of the data window stems from two modeling limitations. First, T_e is generally assumed to be constant within the data windows used, such that if the data encompasses regions with different rigidities, the estimated T_e is a weighted average. Secondly, when the data window is small relative to the flexural wavelength, the T_e estimate tends simultaneously to be biased toward lower values and have larger variance (see *Swain and Kirby* [2003], *Audet and Mareschal* [2004], *Pérez-Gussinyé et al.* [2004], and also section 4.1 for a detailed description). Additionally, techniques used for power spectral estimation affect the wavelength content of the topography and gravity data eventually yielding differences in the absolute values of T_e estimates (see *Ojeda and Whitman* [2002] and *Audet and Mareschal* [2004] for tests with differing spectral estimators and section 3.3 for a detailed description of this effect). Despite this, relative spatial variations of T_e estimates tend to agree between different studies such that the areas found to have highest or lowest T_e will persist for various methodologies. Yet, comparisons of T_e in different regions of a continent benefit from application of a single consistent estimation approach, as is carried out in this paper.

[9] In South America, the terrestrial Bouguer gravity anomaly data coverage is uneven and so most previous studies have been limited to regions where there is adequate data. Most have focused on the Andean domain [*Tassara*, 2005; *Stewart and Watts*, 1997; *Watts et al.*, 1995]. An exception are those of *Mantovani et al.* [2005a], who estimate T_e on the basis of an empirical correlation between tidal forcing and elastic thickness. Another is a recent study by *Tassara et al.* [2007], who used wavelet Bouguer coherence to obtain spatial variations in T_e. The results of these two studies, however, differ markedly: *Mantovani et al.* [2005a] obtained large (T_e > 70 km) estimates over the Andean domain comparable to those in cratonic South America. *Tassara et al.* [2007], on the other hand, found T_e in the Andes to be much lower than over the cratonic interior. This latter study is consistent with forward modeling results of Bouguer anomalies in the Andean domain [*Tassara*, 2005, *Stewart and Watts*, 1997; *Watts et al.*, 1995].

[10] In this paper, we present a new T_e map of South America generated using the coherence between continent-scale grids of Bouguer anomaly and topography data together with a multitaper power spectral estimator. We focus on the results in the stable South American platform, first describing the tectonic domains of cratonic South America, the data sources and processing, and the methodology employed to estimate T_e. We then compare our results to those of *Tassara et al.* [2007] and *Mantovani et al.* [2005a]. Subsequently, we examine the relationship of T_e to terrane age and other proxies for lithospheric structure such as shear wave velocity and heat flow. Finally we discuss the spatial correlation of T_e with intracontinental seismicity and its significance for neotectonic deformation of the continental interior.

2. Tectonic Terranes of the South American Platform

[11] The South American stable platform comprises Archean and Proterozoic terranes amalgamated during the Trans-Amazonian (Paleo-Proterozoic), Late Meso-Proterozoic and the Brasiliano/Pan African orogenies [*Almeida et al.*, 2000] (Figure 1). The supercontinents Atlantica, Rodinia and West Gondwana, respectively, resulted from the culmination of these three tectonic cycles [*Brito Neves et al.*, 1999].

[12] Within the platform, the Amazonian, Sao Francisco and Rio de la Plata cratons are the largest cratonic blocks remnant after these cycles (Figure 1). These blocks contain Archean nuclei as well as fragments of Paleo-Proterozoic and Late Meso-Proterozoic/Early Neo-Proterozoic fold belts [*Brito Neves et al.*, 1999]. The most extensive exposures of Archean rocks are found within the Amazonian and Sao Francisco cratons [*Almeida et al.*, 2000]. The Amazonian craton is divided into the Guyana and Guaporé Shields, which consist of four different geological terranes of Archean and Early/Middle Proterozoic age. The Guyana shield is dissected by a SW-NE trending graben, the Tacutu Mesozoic graben (Figure 1). The graben separates blocks having different composition and age, so probably it is a reactivated structure of Late/Middle-Proterozoic age.

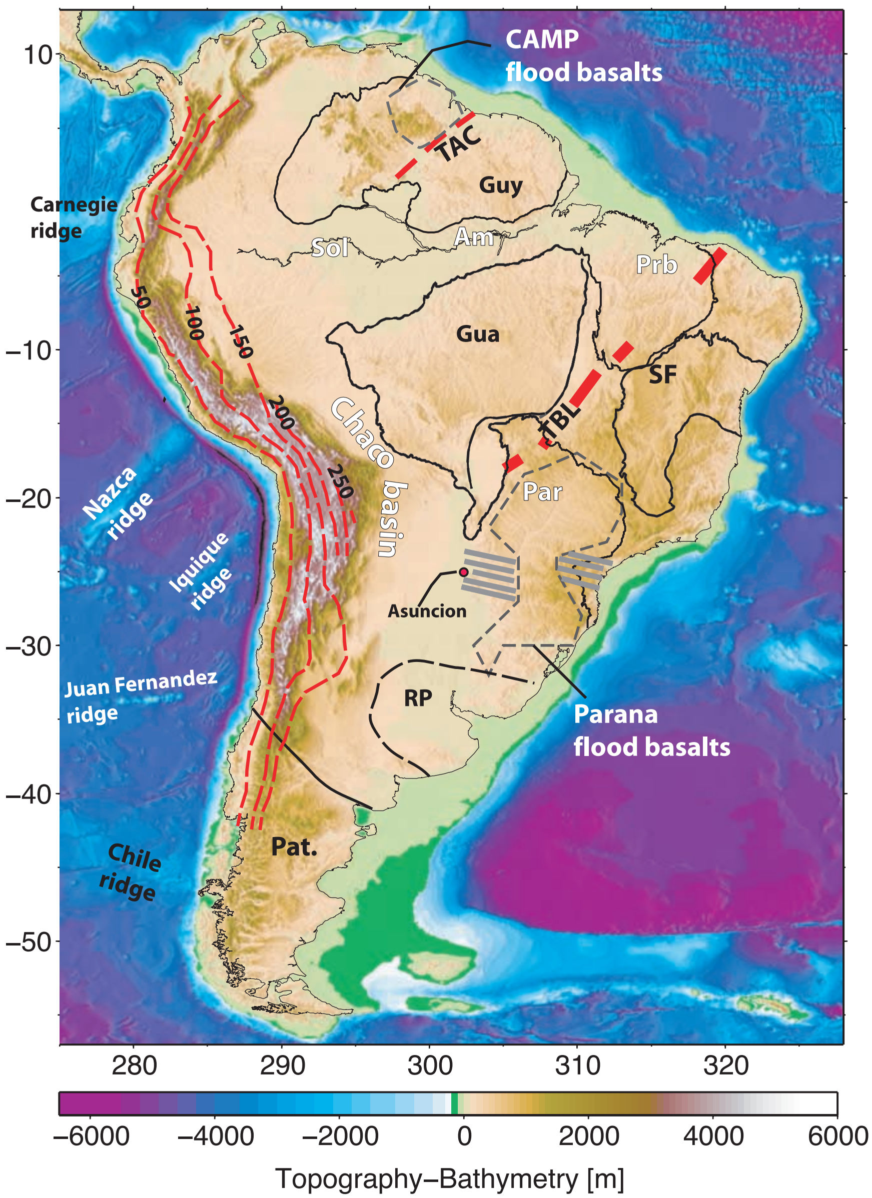

Figure 1. Topography of South America with main tectonic provinces within the stable platform. The Guaporé, Gua, and Guyana, Guy, shields have basement of the same nature and age ranging from Archean to Early/Middle Proterozoic. Together they form the Amazonian craton. Within the Guyana Shield, the Tacutu Mesozoic rift, TAC, is a failed rift branch associated with the opening of the central Atlantic in Lower Jurassic times. Late Triassic flood basalts belonging to the central Atlantic magmatic province (CAMP) are located at the northwestern end of the Tacutu graben (approximate location shown by dashed gray line [*Phipps Morgan et al.*, 2004]), which separates blocks with different Archean and Proterozoic age suggesting an ancient suture that predates central Atlantic opening. TBL is the Transbrasiliano lineament, a continental scale suture that recorded the amalgamation of the Amazonian with the San Francisco, SF, and Rio de la Plata, RP, cratons during the Brasiliano/Pan African cycle. The location of the Rio de la Plata craton is poorly known, and we show it with a black dotted line. The Patagonian terrane, Pat, was amalgamated during the Phanerozoic. The red dot is the location of Asunción in Paraguay, and the gray lines represent dyke swarms that fed the Paraná flood basalts [*Hawkesworth et al.*, 2000]. The extension of the flood basalts is shown with a black dashed line. Par is Paraná basin; Prb is Parnaiba basin. Both basins are thought to be underlain by cratonic lithosphere; see text. Am and Sol are Amazonian basin (east of 300°) and Solimoes basin (west of 300°), respectively. Within the Andean domain, iso-depth contours to the oceanic slab from *Syracuse and Abers* [2006] are shown with red dashed lines; numbers are depths in kilometers.

 10.1029/2006GC001511

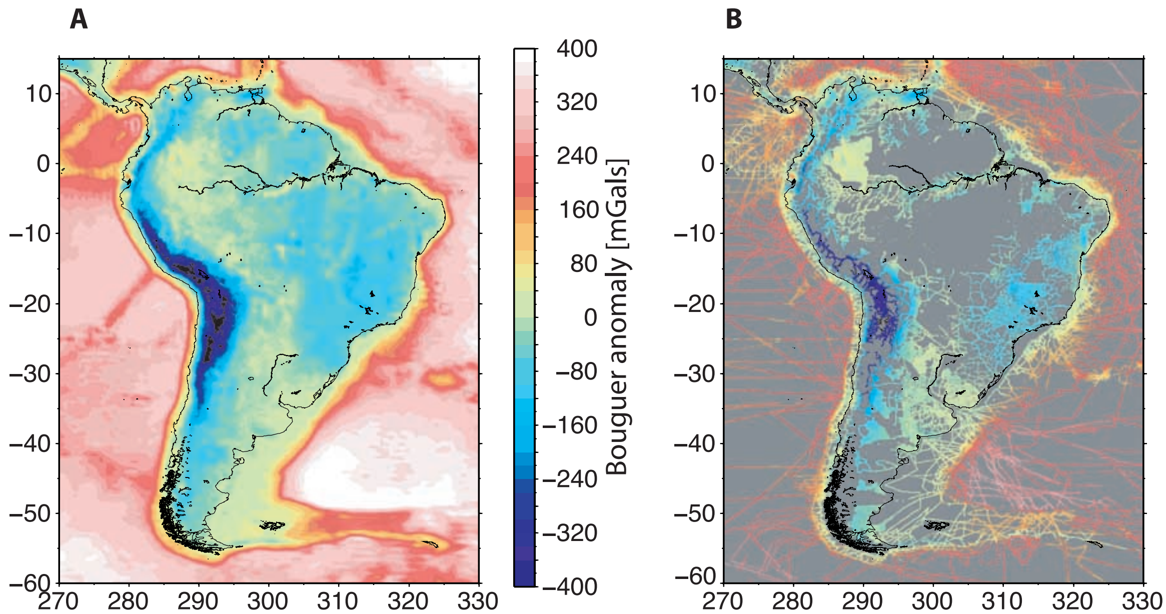

Figure 2. Figure 2a is the final Bouguer anomaly after merging the SAGAP data points shown in Figure 2b with the global model of 1° of resolution: EIGEN-CG30C, obtained from CHAMP and GRACE satellites and terrestrial data [*Foerste et al.*, 2005]. See text for a discussion on the procedure to obtain the Bouguer anomaly.

[13] The collision of the Amazonian craton to the north with the Sao Francisco and Rio de la Plata cratons to the south during the Pan-African/Brasiliano orogeny is recorded by the Transbrasiliano megasuture (Figure 1) [*Cordani and Sato*, 1999]. The suture is a continent-scale NE-SW ductile shear zone that extends into West Africa as the Hoggar suture [*Trompette*, 1994]. In South America the suture extends from northeast Brazil to the Bolivian border (Figure 1) [*Trompette*, 1994].

[14] The Rio de la Plata craton is thought to underlie Paleozoic and Mesozoic sedimentary successions beneath most of southeastern Brazil, Uruguay and northern Argentina [*Trompette*, 1994; *Basei et al.*, 2000]. The approximate location of the craton is shown in Figure 1. The southernmost part of South America is occupied by the Paleozoic Patagonia terrane. This terrane was accreted to the South American stable platform during the Hercynian orogeny, culminating in the amalgamation of Pangea [*Ramos*, 2000].

[15] The South American stable platform includes a number of large Paleozoic basins: the Amazon, Solimoes, Parnaiba, and Paraná in Brazil, and the Chaco in Argentina. The Paraná basin in Brazil comprises Mesozoic basalts that were possibly derived from the Tristan da Cunha hot spot [*Turner et al.*, 1994]. The dyke-swarms that fed the flood basalts have been mapped in Ponta Grossa in Brazil and in a region eastward of Asunción in Paraguay (Figure 1). Despite this magmatic episode, the basin is thought to be underlain by a cratonic block on the basis of radiometric dating [*Cordani et al.*, 1984], Bouguer anomaly studies [*Mantovani et al.*, 2005b] and the high S-velocities that have been imaged to 200 km depth [*Schimmel et al.*, 2003; *Snoke and James*, 1997].

3. Methodology

3.1. Generation of a Continent-Wide Bouguer Anomaly Grid

[16] To produce the continent-wide Bouguer anomaly shown in Figure 2, we have combined irregularly distributed Bouguer gravity anomalies compiled by GETECH as part of their South America Gravity Project (SAGP) [*Green and Fairhead*, 1991] with those derived from free-air gravity anomaly data from the EIGEN-CG30C model. To our knowledge, the compilation presented in this work constitutes the most accurate gravity database used for T_e studies over the whole South American continent. The EIGEN-CG30C data set combines free-air gravity data measured by the satellites CHAMP (860 days) and GRACE (376 days) with various sources of marine and terrestrial free-air gravity including EGM96 to yield a final grid of 1° lateral resolu-

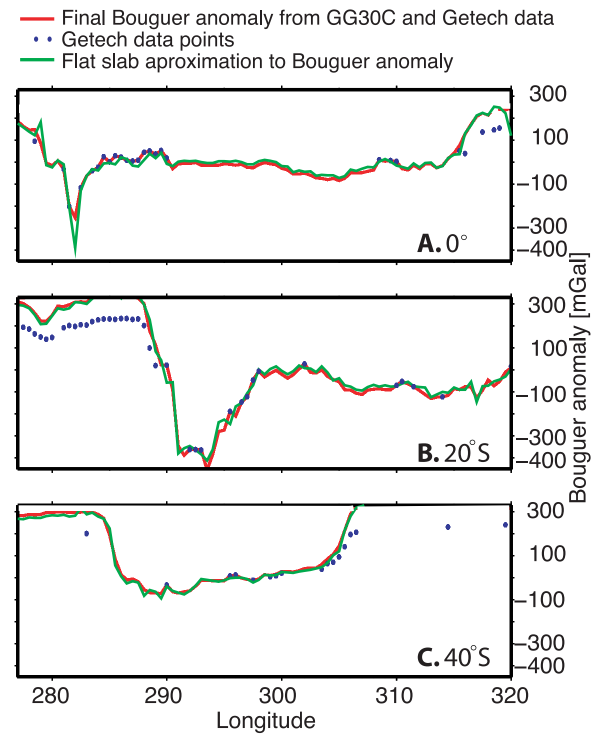

Figure 3. Tracks of the final Bouguer anomaly constructed using a spherical approximation to the Bouguer anomaly (red line) along three different latitudes: (a) 0°, (b) 20°S, and (c) 40°S. The flat slab approximation to the Bouguer anomaly (green line) and the Bouguer SAGAP data points (blue dots) are also shown. Note that in oceans the SAGAP data is free-air anomaly.

tion. The overall accuracy of the EIGEN-CG30C model at spatial scales of ~100 km is estimated to be 8 mgal [*Foerste et al.*, 2005].

[17] The coherence function used here to calculate T_e, estimates the correlation of topography and Bouguer gravity anomaly as a function of wavelength. Subsequently, the coherence is modeled to determine the effective elastic thickness of the lithosphere. Therefore, to avoid introducing spurious wavelengths in the Bouguer anomalies and thereby noise in the coherence function, the topography used for the Bouguer correction must have the same resolution as that of the free-air gravity grid. Given that the EIGEN-CG30C free-air gravity grid has a resolution of 1° and the length of a longitudinal degree varies by ~60% from northern to southern South America, one cannot define a wavelength in planar coordinates equivalent to 1° of resolution over the entire continent. Therefore we transformed a topography grid to spherical coordinates and calculated the Bouguer correction, $\Delta g(r, \theta, \phi)$ to 1° resolution following *Wieczorek and Phillips* [1998] and *Lowry and Zhong* [2003]:

$$\Delta g(r,\theta,\phi) = \frac{(l+1)GM}{r}\sum_{ilm}\left(\frac{D}{r}\right)^{l+1} C_{ilm}Y_{ilm}(\theta,\phi)$$

$$C_{ilm} = \frac{4\pi\Delta\rho D^2}{M(2l+1)}\sum_{n=1}^{l+3}\left[\frac{{}^{n}h_{ilm}}{D^n n!}\frac{\prod_{j=1}^{n}(l+4-j)}{(l+3)}\right]$$

These equations yield the gravity anomaly, $\Delta g(r, \theta, \phi)$, due to a topographic surface, $H(r, \theta, \phi)$, referenced to a sphere of radius D, and are the spherical equivalent to Parker's finite-amplitude formulation of gravity due to topography on a plane [*Parker*, 1972]. Here are the harmonic coefficients corresponding to the spherical transform of the nth power of the topography, M is mass of the Earth and G is the universal gravitational constant.

[18] Finally, the Bouguer anomaly derived from the EIGEN-CG30C data was merged with the sparsely distributed GETECH Bouguer anomaly to obtain the final grid. The two data sets were combined such that EIGEN-CG30C data were replaced by GETECH data points where available. The final grid spacing is 8 km, although the information content generally corresponds to the 1° grid outside of areas where dense GETECH data are available (Figure 2). Before merging we tested for systematic offsets between the two data sets. Figure 3 shows the GETECH data (blue circles), the profiles of the Bouguer anomaly constructed using the spherical Bouguer correction (in red), and the profiles of the Bouguer anomaly using a slab correction (in green). The GETECH data points offshore are free-air anomalies, so are systematically lower than our final Bouguer anomaly offshore (Figure 3), but the onshore anomalies are in close agreement.

[19] Our T_e analysis is implemented in Cartesian coordinates, necessitating a projection of the spherical data that minimizes distortion. We accomplished this by dividing South America into four smaller grids north-to-south and projecting to planar coordinates within each area. We then back-projected the Cartesian-coordinate T_e maps into longitude and latitude for presentation.

3.2. Bouguer Coherence Using a Multitaper Spectral Estimator

[20] The effective elastic thickness, T_e, of the lithosphere is the thickness of an ideal elastic plate

10.1029/2006GC001511

that would bend by the same amount as the lithosphere, under the same applied loads [e.g., *Watts*, 2001]. Because layers composing the lithosphere fail anelastically, the measured T_e is actually an integral of the elastic bending stress, constrained by the limits imposed by the brittle and ductile rheologies of the lithosphere [*Burov and Diament*, 1995; *Lowry and Smith*, 1995].

[21] To measure the elastic thickness, we use as input data the topography (which sums surface loads imposed on the lithosphere and the flexural deflections that compensate both surface and subsurface loads), and the Bouguer anomaly (which contains the mass signal from subsurface loads plus the deflections caused by loading). The coherence function between the topography and Bouguer anomaly, commonly known as Bouguer coherence, gives information on the wavelength band over which topography and Bouguer anomaly are correlated, and is given by

$$\gamma^2_{obs} = \left\langle \frac{|S_{hb}(k)|^2}{S_{hh}(k)S_{bb}(k)} \right\rangle$$

where S_{hb} (k), S_{hh} (k), S_{bb} (k) are the cross-power spectrum of the topography and Bouguer anomaly and the auto-power spectra of the topography and of the Bouguer anomaly, respectively. Angle brackets denote averaging over annular wave number bands of the wave number modulus $k = |k| = \sqrt{k_x^2 + k_y^2}$.

[22] The Bouguer coherence generally tends to zero at short wavelengths, where the topography is not compensated, and it tends to one at long wavelengths where the response to loading is Airy-like [*Forsyth*, 1985]. The wavelengths at which the coherence increases from 0 to 1 depend on the effective elastic thickness, T_e, of the lithosphere. When the lithosphere is relatively weak and T_e is small, local compensation for loading occurs at relatively shorter wavelengths.

[23] To estimate T_e, we compare the observed coherence with the coherence curves predicted for a particular set of T_e values. The T_e that minimizes the difference between the predicted and observed coherence is the assigned T_e for an analyzed area. To calculate the predicted coherence, assumptions about the loading processes in the lithosphere need to be made. We follow *Forsyth* [1985] and assume that surface loads (atop the lithosphere) and subsurface loads (within the lithosphere) are statistically uncorrelated. Surface loads include the thrust sheets that comprise topography in orogenic belts while subsurface loads include intracrustal thrusts and magmatic underplating. For any given T_e, we calculate a set of surface and sub-surface loads and compensating deflections that reproduce exactly the observed topography and gravity anomaly, an approach commonly known as load deconvolution [*Forsyth*, 1985]. Using this approach, the ratio of surface to subsurface loads, or loading ratio, varies with two-dimensional wave number and is not imposed as an independent parameter as when analytical solutions are calculated.

[24] *Forsyth*'s [1985] original formulation of the predicted coherence assumes that all internal density variation and loading occurs at the Moho. We used CRUST2.0 [*Bassin et al.*, 2000] to define the internal density profile and assumed that internal loading occurs at the interface between upper and mid-crust. The lateral variation in depth of this interface was obtained from CRUST2.0. Since the observed coherence can be reproduced equally well by either low T_e and shallow loading or a larger T_e and deeper loading, there is a trade-off between T_e and assumed depth of loading. However, we tested the sensitivity of Te to loading depth in Europe and found that changing the loading depth from the mid-crust to Moho changed T_e by ~5 km, but the general patterns of variations remained the same [*Pérez-Gussinyé and Watts*, 2005].

[25] Although we do not explicitly include the subducting Pacific slab in our loading model, modeling of the slab Bouguer anomaly signal expected for the ≥100 km depth contours shown in Figure 1 indicates that signal is dominated by wavelengths that are much longer than the wavelengths of flexural transition or even the window dimensions used in this analysis. The subducting slab correlates with the ~2000 km long-wavelength anomalies of the Bouguer anomaly field (but has opposite sign, such that main effect of the slab is to offset the gravity signal associated with thickened crust in the Andean plateau by 5−10%). The longest wavelength used for analysis here is ≤800 km, corresponding to the largest window dimension. Hence, at wavelengths of the flexural transition, slab dynamical effects in gravity and topography change the coherence of the two negligibly. Re-estimation of T_e after subtracting the estimated slab signal from the Bouguer data yields a negligible change in the estimates [*Pérez-Gussinyé et al.*, 2006].

3.3. Resolution Tests With Synthetic Data

[26] Calculation of the observed and predicted coherence involves transformation into the Fourier domain of the topography and Bouguer gravity anomaly to estimate their auto- and cross-power spectra. Because both data sets are non-periodic and finite, the Fourier transformation presents problems of leakage, or transference of power between neighboring frequencies, resulting in estimated spectra that differ from the true spectra. To reduce leakage, the data are tapered prior to Fourier transformation. However, ultimately, the type of taper used influences slightly the resulting power spectra and hence the coherence function. Hence the ability to recover T_e differs depending on the tapering technique used, making it important to understand its limitations.

[27] In this paper, we use Thomson's multitaper method [*Thompson*, 1982] with Slepian windows [*Slepian*, 1978]. The spectral estimator obtained with the multitaper is a weighted average of the spectra generated with a set of individual, orthogonal tapers. The multitaper estimator reduces the variance of the spectral estimate and also defines spectral resolution [*Percival and Walden*, 1993]. The set of orthogonal tapers are defined by setting the bandwidth of the central lobe of the power spectral density of the first-order taper, W. For a given W, there are a maximum of K = 2NW − 1 number of tapers, with good leakage properties that can be used for the estimation of the spectra, where N is the number of samples within the data window [e.g., *Percival and Walden*, 1993; *Simons et al.*, 2000]. Variance of the spectral estimates decreases with the number of tapers used as 1/K, so that the bandwidth and number of tapers are chosen depending on the function under analysis [*Percival and Walden*, 1993]. We use here a multitaper scheme corresponding to NW = 3, which is also used in many other studies for T_e estimation [e.g., *Audet and Mareschal*, 2004; *Pérez-Gussinyé et al.*, 2004; *Pérez-Gussinyé and Watts*, 2005]. Additionally, we deconvolve the loads within the same data window as was used to derive the observed coherence. *Pérez-Gussinyé et al.* [2004] deconvolved loads in a window larger than that used to calculate the observed coherence/admittance. Subsequently, the loads resulting from the deconvolution were transformed back into the spatial domain and windowed within the same region and multitaper parameters as the observed coherence/admittance. Here we have deconvolved the loads and calculated the power spectra within the same window to speed up the calculation of T_e. We show here tests with synthetic data of the method's ability to recover T_e using this slight variation on the method. These tests indicate that estimation bias and variance similar to those given by *Pérez-Gussinyé et al.* [2004] can be achieved using smaller T_e estimation windows.

[28] The generation of synthetic data has been explained in detail by *Pérez-Gussinyé et al.* [2004] and will only be briefly described here. The synthetic topography and gravity data was generated by placing uncorrelated surface and subsurface mass loads on an elastic plate using an algorithm similar to that of *Macario et al.* [1995]. First, the Fourier amplitudes of uncorrelated surface, Hi, (k), and subsurface, Wi, (k), mass loads were calculated imposing that their spectra follows a power law distribution with respect to wave number, with a fractal dimension of 2.5, as it is observed for the amplitude spectra of the real topography [*Mandelbrot*, 1983; *Turcotte*, 1997]. Surface and subsurface loads were then standardized (unit variance) and their amplitudes were scaled so that their loading ratio has an expected value of 1, although the loading ratio varies with wave number. Vertical stresses ρ_cgHi and $(\rho_m - \rho_c)$gWi, where g is gravitational acceleration and ρ_c and ρ_m are the densities of the crust and mantle respectively, were applied as loads at the surface and Moho, respectively, of a thin elastic plate with a specified elastic thickness T_e. In the case where T_e is spatially constant, the amplitudes of the final topography, H, and Moho deflection, W, were calculated from the load response relations given in Appendix A of *Pérez-Gussinyé et al.* [2004]. The Bouguer anomaly was calculated from the Moho deflection using the *Parker* [1972] finite amplitude formulation up to a fourth-order approximation. We computed 100 such sets of topography and Bouguer anomaly by changing the random generator seed.

[29] In Figure 4 we show tests of synthetic topography and Bouguer anomaly generated with a spatially constant *Te* and multitaper parameters of NW = 3 and K = 5 (as done by *Pérez-Gussinyé et al.* [2004]). The grid interval is 8 km. The tests show that when the flexural wavelength, $\lambda = \pi(4D/\Delta\rho g)^{1/4} \sim 29\ T_e^{3/4}$ [*Swain and Kirby*, 2003], is large relative to the window size, some of the resulting *Te* values are underestimated and that additionally, the number of spuriously high *Te* estimates, or outliers, increases (as previously observed by *Swain and Kirby* [2003], *Audet and Mareschal* [2004], and *Pérez-Gussinyé et al.*

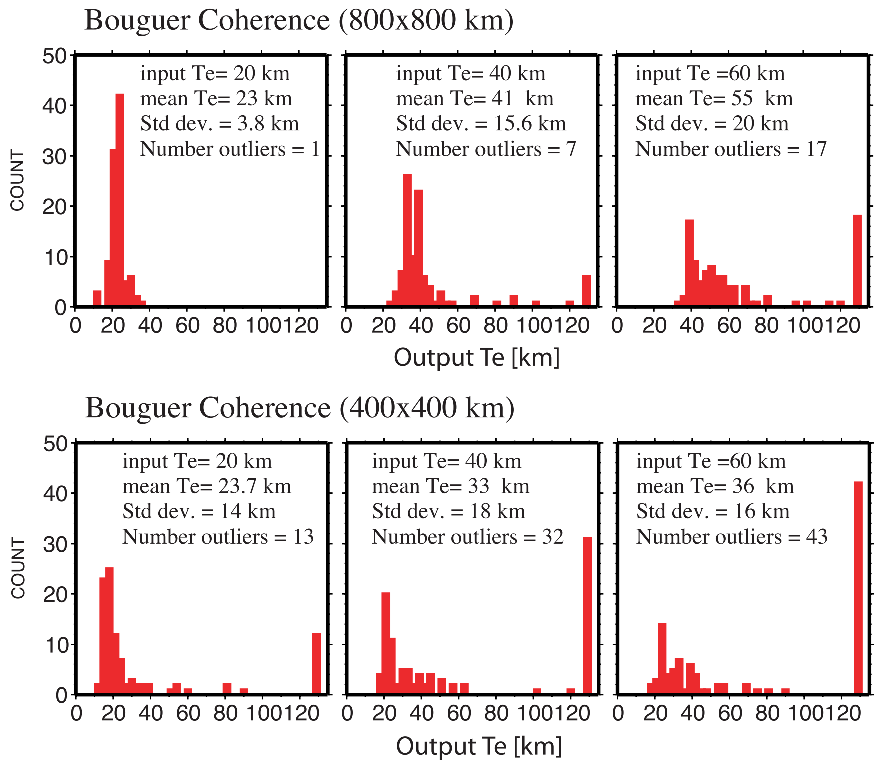

Figure 4. Tests with synthetic data and constant T_e for (top) 800 × 800 km windows and (bottom) 400 × 400 km windows. The synthetic data used are the same as those used by *Pérez-Gussinyé et al.* [2004], but the tests shown here used smaller windows and a different load deconvolution routine (see section 3.3). The legend details the input T_e value, the mean output T_e, standard deviation, and number of outliers for 100 tests. Note that for a window of a given size, the number of outliers (defined as $T_e > 120$ km) increases as the true T_e increases.

[2004]). Therefore, when T_e is constant, larger windows produce more accurate estimates.

[30] However, T_e is likely to vary in different geological terranes. To generate synthetic data with spatially varying T_e, we transformed the initial surface and subsurface loads to the spatial domain and solved the fourth-order flexural governing equation using a finite difference solution [*Wyer*, 2003; *Stewart*, 1998]. In order to retrieve a spatially varying T_e structure, the T_e analysis was carried out using constant sized, overlapping windows with centers spaced 56 km apart. Within each window T_e was assumed to be constant, and the T_e estimate was assigned to its center.

[31] Figure 5 shows estimates from synthetic data generated with the spatially varying structure shown in Figure 5d, using multitaper parameters NW = 3 and K = 5 and three different windows of 400 × 400 km, 600 × 600 km and 800 × 800 km (see *Pérez-Gussinyé et al.* [2004] for results with larger windows). For the smallest window, the values toward the centre are overestimated and those around the high T_e nuclei are underestimated (Figure 5c). The 600 × 600 km window recovers the spatial variations better although it still overestimates the highest T_e values (Figure 5b). Finally, the larger window size recovers the highest T_e values better but overestimates the lower T_e values due to spatial averaging (Figure 5a). Hence there is a trade-off between spatial resolution, which ideally would be better with smaller windows, and the ability to recover large T_e values, which should improve with larger windows [see also *Pérez-Gussinyé et al.*, 2004]. Here we choose to use a Fourier windowing technique based on the multitaper and analyze the T_e in South America using 3 different window sizes.

[32] To estimate T_e in South America we did several tests with different NW values and number of tapers. The pattern of T_e variation is similar with the different multitaper parameters used, but the mean values change, as they do when the window size changes (see Figure 5). Here, we present the results for NW = 3 and 5 tapers for all of South

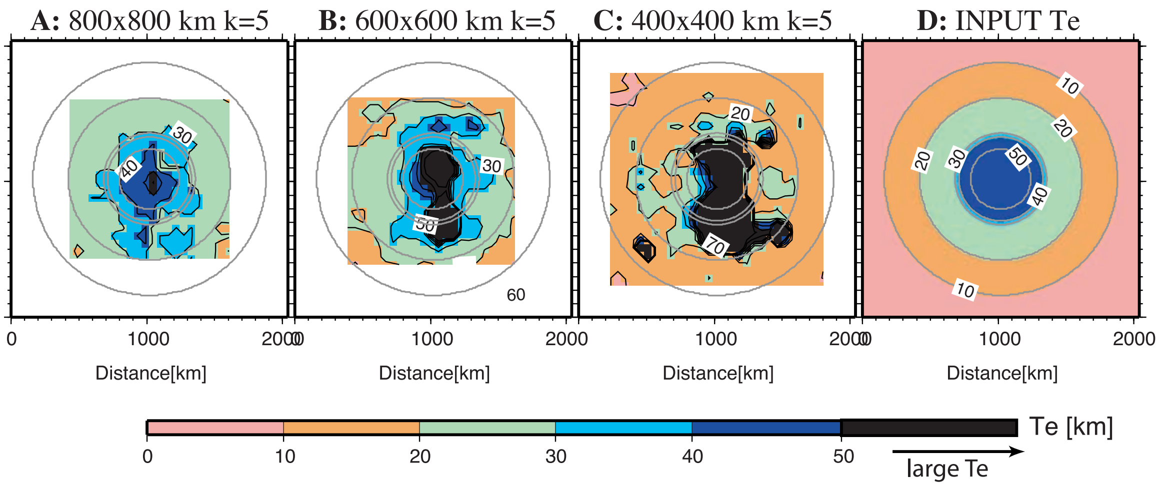

Figure 5. Recovery of the variable T_e structure shown in Figure 5d, using windows of different sizes. The synthetic data are generated as those used by *Pérez-Gussinyé et al.* [2004]. (a) 800 × 800 km, (b) 600 × 600 km, and (c) 400 × 400 km. Multitaper parameters are NW = 3 and K = 5 (see section 3.3 for the meaning of these parameters). Gray circles in Figures 5a, 5b, and 5c represent the contoured T_e values shown in Figure 5d. The smallest windows, Figure 5c, tend to overestimate the largest T_e values (50 km) and underestimate intermediate T_e values ranging from 20 to 30 km. The largest windows, Figure 5a, approximate the largest T_e better but overestimate T_e < 20 km due to spatial smearing and averaging (see text for a detailed description and also *Pérez-Gussinyé et al.* [2004] for similar tests with larger windows).

America (Figure 6). We have chosen these parameters because the larger number of tapers gives a relatively smooth solution over stable South America. In this area the topography has low relief, so that errors and dynamical noise fields in the topography and gravity data can have relatively greater effect on the coherence of the two data sets. Consequently, it is important to have stable (small variance) power spectral estimates, which implies the use of 5 tapers, the maximum allowed for NW = 3 (note that the variance in the spectra decreases with 1 over the number of tapers). We have performed tests with 3 tapers and small windows (400 × 400 km) over the stable platform, and found that this combination of taper parameters and window size is unstable, as it produces large variance in the coherence estimates, making it difficult to differentiate between real geological structure and noise in the T_e estimates. Therefore we use a larger number of tapers, to obtain a smooth T_e structure even with small windows, which allows having a detailed lateral resolution of the structures within the stable platform (Figure 6a).

4. Results

[33] We have estimated T_e using windows of 400 × 400 km, 600 × 600 km and 800 × 800 km. Since large T_e values cannot be recovered with confidence using such small windows, we plot T_e > 70 km in black in Figure 6. Our results show a first-order T_e variation in South America in which the Andes have relatively low T_e and the stable platform has relatively high values (Figure 6). Although the first-order pattern of spatial variation in T_e remains similar for the three estimation windows, there are differences in the lateral extent of the imaged structures as well as the mean T_e recovered. These differences are analogous to those observed when synthetic data are used (Figures 4 and 5). For example, within the predominantly high T_e stable platform, areas of low T_e are more prominent with the smallest windows, as these image lateral boundaries in T_e better. This is because larger windows spatially average small areas with low T_e embedded within areas with large T_e such that they may be damped or disappear entirely. For example, compare the relatively low T_e area along the Transbrasiliano lineament in Figures 6a and 6c.

[34] Along the Andean orogenic belt and flanking foreland, T_e also changes considerably with window size. For example, along the Andean foreland there is an area of high T_e, centered at ∼65°W and 18°S, which has an arcuate shape and is clearly distinguished in the 800 × 800 km and 600 × 600 km window results (Figures 6b and 6c) but is

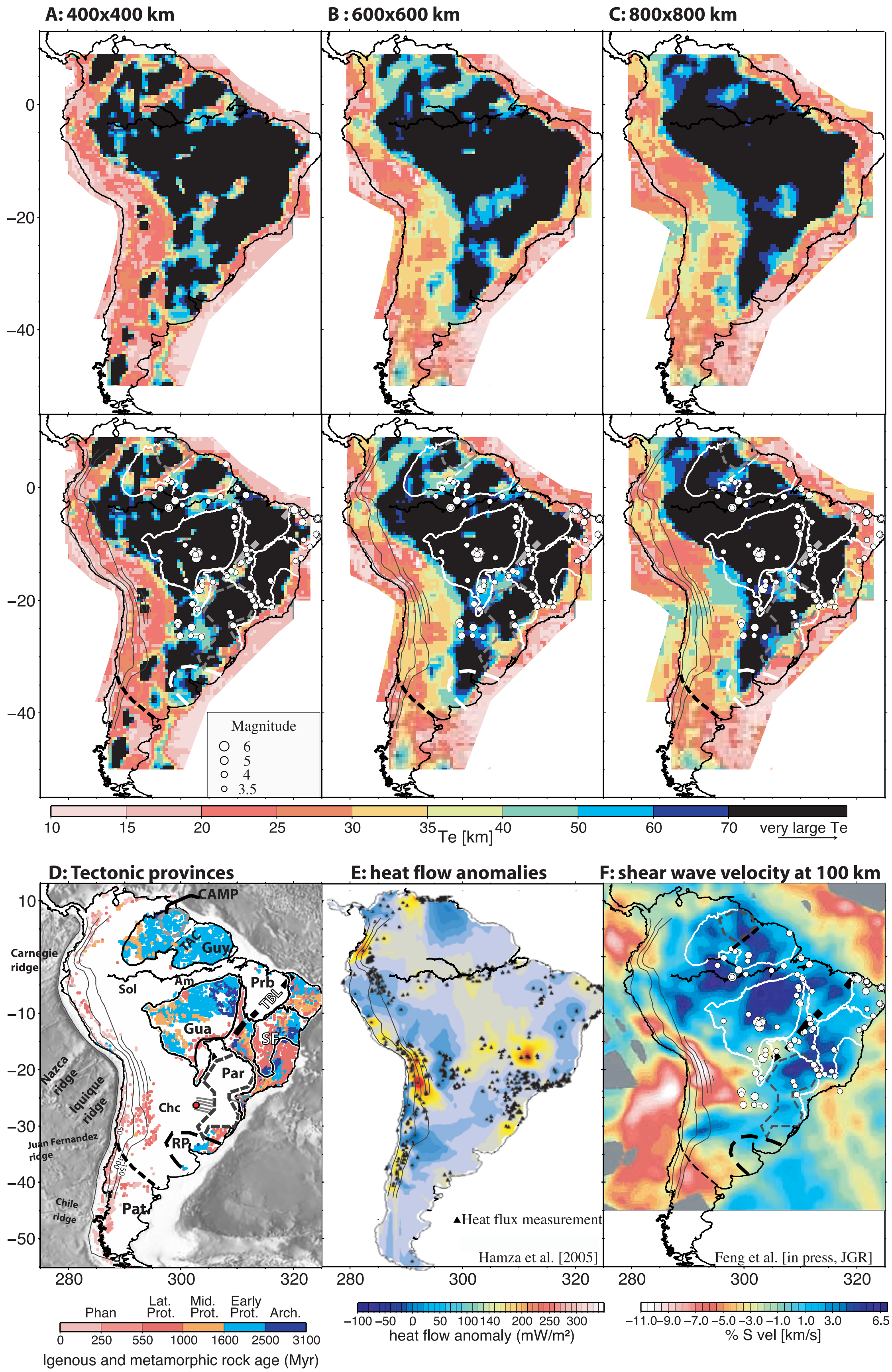
A: 400x400 km
B : 600x600 km
C: 800x800 km
Magnitude
6
5
4
3.5
Te [km]
very large Te
D: Tectonic provinces
E: heat flow anomalies
F: shear wave velocity at 100 km
CAMP
Carnegie ridge
Nazca ridge
Iquique ridge
Juan Fernandez ridge
Chile ridge
TAC
Guy
Sol
Am
Prb
TBL
Gua
SF
Par
Chc
RP
Pat
Phan
Lat. Prot.
Mid. Prot.
Early Prot.
Arch.
Igenous and metamorphic rock age (Myr)
▲Heat flux measurement
Hamza et al. [2005]
heat flow anomaly (mW/m²)
Feng et al. [in press, JGR]
% S vel [km/s]

Figure 6

nearly invisible in the 400 × 400 km estimates (Figure 6a). We interpret that the high T_e observed in the 800 × 800 km and 600 × 600 km windows reflects a relatively strong part of the Brazilian Shield that underthrusts the sub-Andean fold and thrust belt. Our interpretation is based, in part, on previous 1-D analysis along the Andean foreland in the bend region which observed a similar structure [*Stewart and Watts*, 1997; *Watts et al.*, 1995]. Local tomography in the vicinity of 16°S also exhibits a strong lateral change in P wave velocity beneath the Eastern Cordillera (~65.5°W), with high velocities to the east interpreted as underthrusting craton [*Dorbath et al.*, 1993]. Shear wave anisotropy studies also show a change of the fast propagation direction from north-south to east-west, consistent flow patterns expected if the edge of the cratonic lithosphere is at ~ 65.5°W [*Polet et al.*, 2000]. Thus we believe that the 400 × 400 km window results miss part of the actual T_e structure in this area. Two localized patches of very high T_e (>70 km) are observed in the small window estimates for this area. We interpret that these high rigidities occur because the flexural wavelength is large in relation to the window, and the rest of the T_e values are underestimated here similar to what we observe in Figures 4 and 5.

[35] Despite the differences in estimates of T_e along the Andean chain, some relative T_e variations are common to all three estimation windows. These include: increasing rigidity from 40°S to ~20°S in the region overlying the 50 to ~100 km depth contours to the subducting slab, and comparatively lower rigidity in continental lithosphere overlying the subducted Nazca and Carnegie ridges (Figure 6). In subsequent work we detail window and multitaper estimation parameters, which best describe the lateral variation of T_e in the Andean domain. There, the significance of these variations for the thermal and mechanical structure and the geodynamics of the Andean domain will be discussed (M. Pérez-Gussinyé et al., Spatial variations in the effective elastic thickness, T_e, along the Andes: Implications for subduction geometry, manuscript in preparation, 2007; hereinafter referred to as Pérez-Gussinyé et al., manuscript in preparation, 2007). In the next section we compare our results with previous studies. Subsequently, we discuss the relationship of T_e to the tectonic, seismic and thermal structure of the stable platform as well as its significance for neotectonic deformation of the continental interior.

4.1. Comparison With Previous Results

[36] Previous estimates of T_e for the entire continent of South America include those of *Mantovani et al.* [2001, 2005a] and *Tassara et al.* [2007]. Our results are in agreement with the findings of *Tassara et al.* [2007] and with forward modeling of Bouguer anomalies along profiles of the Andean domain [*Tassara*, 2005; *Stewart and Watts*, 1997; *Watts et al.*, 1995], all of which indicate that T_e in the Andes is much lower than over the cratonic interior. However, they differ markedly from those of *Mantovani et al.* [2001, 2005a], which indicate large T_e (~70–80 km) over the Andean domain, comparable to estimates in cratonic South America. *Mantovani et al.* [2001, 2005a] estimated T_e using an empirical correlation between tidal gravity anomalies and elastic thickness, and used this correlation to generate elastic thickness values where terrestrial gravity measurements where sparse. Given that tidal loading is of short duration (about one day), and the lithospheric deformation in response to such short-term cyclical stress is quite different than to longer-term geological pro-

Figure 6. (top) T_e estimates for South America for three different window sizes, (a) 400 × 400 km, (b) 600 × 600 km, and (c) 800 × 800 km, and multitaper parameters of NW = 3 and 5 tapers. (Note that black colors indicate indeterminately large T_e). (bottom) The same as in top, but T_e is superimposed by a normalized catalogue of earthquakes within Brazil, Paraguay, and Uruguay (see *Assumpçao et al.* [2004] for a description of the normalization), by the depths to subducted slab (50 to 250 km from *Syracuse and Abers* [2006]) and by the main tectonic provinces. (d) Bathymetry of South America offshore, and the age of igneous and metamorphic rocks believed to indicate the age of crustal formation [*Schobbenhaus and Bellizia*, 2001]. These are overlain by the main tectonic provinces and the depths to the slab [*Syracuse and Abers*, 2006]. Abbreviations are as in Figure 1, except for Chc, which is Chaco basin. (e) Heat flow anomaly which results from subtracting a regional heat flow field from the observed heat flow values [*Hamza et al.*, 2005]. Triangles are heat flow measurements. The regional heat flow field is a polynomial representation of the South American heat flow and is meant to represent the first-order increase of 60 mW/m^2 in the Stable Platform to 70 mW/m^2 in the Andes [*Hamza et al.*, 2005]. The heat flow anomaly is superimposed by the depths to the slab [*Syracuse and Abers*, 2006]. (f) Shear wave velocity at 100 km depth (from Feng et al., submitted manuscript, 2007) superimposed by the tectonic provinces, the seismicity from the normalized catalogue, and the depths to the slab [*Syracuse and Abers*, 2006].

cesses modeled here [*Willett et al.*, 1984, 1985], the T_e estimates of *Mantovani et al.* [2001, 2005a] are unlikely to be comparable to those estimated here. Moreover, the correlation analysis of tidal gravity anomalies and T_e used by *Mantovani et al.* [2001, 2005a] utilized the very few South American T_e measurements that were available at that time, and this may have biased their results.

[37] The study of *Tassara et al.* [2007] used Bouguer coherence to estimate T_e, and thus their results are directly comparable to ours. One difference between their analysis and ours is that their Bouguer gravity anomaly was derived from the EIGEN-CG30C data set, which was combined in this work with the terrestrial GETECH data to obtain a more detailed data set. An additional important difference is that they used wavelets to find the spatial variations in T_e, while we used a Fourier windowing scheme with the multitaper method. When estimating spatially varying T_e using a data-windowing approach, we are faced with the dilemma that the small windows that would best resolve spatial variability in T_e cannot recover large elastic thicknesses. However, larger windows that adequately recover high T_e values tend to smooth out lateral contrasts in T_e, yielding a spatially smoothed version of the underlying T_e distribution. The window size restricts the largest T_e that can be recovered with confidence, in our case $\sim$70 km.

[38] In this study, we circumnavigate the problem of choosing an optimal window by presenting results for different window sizes and interpreting them according to the results obtained with synthetic data. *Tassara et al.* [2007] chose the alternative approach of using a wavelet transform to estimate a local coherence function at each point of the data grid (an approach originally developed by *Kirby and Swain* [2004], *Kirby* [2005], and *Swain and Kirby* [2006]). To perform the wavelet transform, the signal (e.g., topography or gravity anomaly) is convolved with a family of wavelets, which have a range of dimensions, or scales (for a more detailed description, see *Kirby and Swain* [2004]). Small-scale wavelets reveal the short-wavelength information content of the data, while large-scale wavelets reflect long-wavelength information [*Swain and Kirby*, 2006]. Convolution effectively yields a wavelet transform estimate at every node of the data grid, enabling construction of wavelet cross- and auto-power scalograms (the wavelet equivalent to the Fourier domain cross- and auto-power spectra), and hence the wavelet coherence, at each data node and for each wavelet scale [*Kirby and Swain*, 2004]. Because scale can be mapped to wave number, the wavelet coherence can be represented also as a function of the latter [*Kirby and Swain*, 2004].

[39] Thus, ideally, the wavelet transform method would solve the dilemma of the choice of window size by essentially using a different window for each wave number and location [*Kirby and Swain*, 2004]. However, the T_e estimates of *Tassara et al.* [2007] have a much smoother appearance than those presented in this paper. For example, the results presented here and those of *Tassara et al.* [2007] both show the southwestern part of the Transbrasiliano lineament to have low T_e (compare Figures 6a and 6b with Figure 3 of *Tassara et al.* [2007]). In our results, the low T_e area continues along trend to the north, while the wavelet method does not resolve this northward continuation, similar to what occurs when we use large windows (Figure 6c). Likewise, the area west of the Paraná flood basalts, the Amazon basin and the Tacutu graben appear as clear lineaments of low T_e in our results (Figure 6a and partly Figure 6b) but are not distinguished in the work of *Tassara et al.* [2007].

[40] Hence, despite similarities in the loading models used, our results and those of *Tassara et al.* [2007] differ markedly in the resolution of the low T_e areas within the stable continent, raising the obvious question of why. Differences between our results and those of *Tassara et al.* [2007] could be attributed to some combination of (1) the greater information content of the gravity anomaly data used in our analysis, (2) greater variance of multitaper windowed T_e estimates when the window is not much larger than the wavelength of flexural transition, and (3) reduction of information content in the wavelet analysis of *Tassara et al.* [2007] by inverse-wave number weighting of the norm of predicted minus observed coherence.

[41] In order to test whether the greater accuracy of the Bouguer anomaly data used here relative to that used by *Tassara et al.* [2007] could explain the differences in the results, we have re-computed T_e using only the EIGEN-CG30C. Figure 7 shows that the low T_e area in the Amazonian basin is less pronounced using only EIGEN-CG30C data. However, other low T_e areas within the continental interior are very similar in extent using both data sets. This suggests that the greater information content of the Bouguer data used here cannot by itself account for the difference in the results.

10.1029/2006GC001511

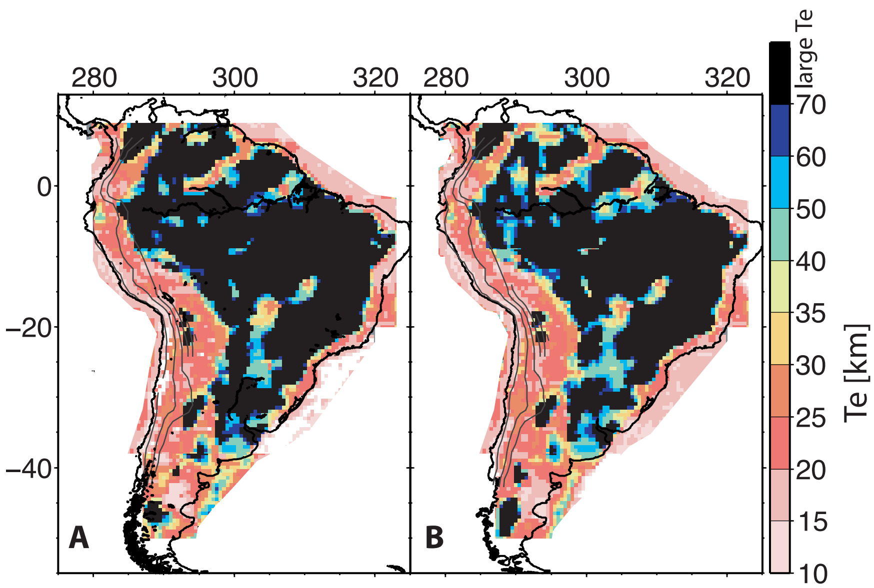

Figure 7. T_e of South America estimated using 400 × 400 km windows and (a) the Bouguer gravity anomaly derived only from the EIGEN-CG30C data. (b) The same as in Figure 7 but using the data generated for this study (see section 3.1). These data result from combining the EIGEN-CG30C-derived Bouguer anomaly and the more detailed SAGAP Bouguer anomaly.

[42] Alternatively, one might interpret that the windowed multitaper spectral approach has greater variance and that many of the low T_e patterns in Figure 6 are spurious. We deem this unlikely, however, given the correlation of low T_e with intracontinental seismicity and regions of greater geological strain (see section 5). Similar correlations have been observed elsewhere [e.g., *Lowry and Smith*, 1995] and are consistent with model predictions of deformation focusing in regions of thin lithosphere and/or low-viscosity upper mantle [e.g., *Latychev et al.*, 2005]. This coupled with the fact that many of these features are persistent, albeit attenuated, in estimates using all three window sizes suggests that they represent real variations in lithospheric flexural rigidity. Indeed, the *Tassara et al.* [2007] estimates are most similar to those we attain when using the largest window size (Figure 6c), which yields a spatially smoothed version of the weak T_e lineaments observed within the cratonic interior (Figure 6a).

[43] The wavelet method used by *Swain and Kirby* [2006] and *Tassara et al.* [2007] weighted the misfit between predicted and observed coherence functions by the inverse wave number in order to downweight the spurious high coherence at large wave numbers that can result from an unrepresentative Bouguer reduction density or from certain algorithms for generating gravity anomalies. On the other hand, the wavelet approach includes a range of wavelet scales that significantly exceeds the wavelength of flexural transition. Including large-scale wavelets in the coherence analysis is somewhat analogous to using large windows in a windowed spectral approach, and while the practice of upweighting the longest wavelengths does reduce the incidence of spurious low T_e estimates, the greater emphasis placed on information contained in the longest wavelengths of the data also tends to smooth fine-scale structure (C. Swain, personal communication, 2007).

[44] Despite their differences, multitaper and wavelet estimates can be complementary if their respective limitations are considered when interpreting the results. While we believe that we attain higher spatial resolution of the low T_e features within the rigid cratonic interior, the *Tassara et al.* [2007] estimates better resolve T_e variations when $T_e >$ 70 km, allowing them to assess which regions have the greatest rigidity within the continent. In future, we plan a more rigorous comparison of the methods using synthetic data.

5. Discussion

5.1. *Te* and Tectonic Provinces

[45] Within the stable platform, T_e values are generally high (>70 km). The figures show that high T_e prevails over most of the Guaporé, Guyana

and Sao Francisco cratons (Figure 6), which largely consist of Archean to Paleoproterozoic basement [*Trompette*, 1994]. High T_e is also found in the Parnaiba and Paraná basins. Radiometric ages of basement samples and the geometry of the surrounding fold belts indicate these basins to be cored by very old (> 2 Ga) basement [*Cordani et al.*, 1984; *Brito Neves et al.*, 1984]. Relatively large T_e has also been estimated from Bouguer coherence by *Vidotti* [1997] and *Vidotti et al.* [1998] in the Paraná and Parnaiba basins using regional gravity anomaly grids. Large T_e is also found in the approximate area of the Rio de la Plata craton (Figure 6). Most of the Rio de la Plata craton is overlain by younger sedimentary sequences of the southern Paraná and southwestern Chaco basins, where its basement is of unknown age, but the few exposures that are found are Archean in age [*Trompette*, 1994].

[46] In the southern part of the stable continent, south of the Patagonian suture, T_e is generally low and the basement is Paleozoic in age (Figure 6). Thus, in South America, the rigidity of terranes which are mainly Archean to Paleo/Middle-Proterozoic appears, in general, to be much larger than that of Phanerozoic terranes, which is consistent with observations made on the European lithosphere [*Pérez-Gussinyé and Watts*, 2005]. Conductive cooling alone cannot explain the difference in *Te* between these terranes, as the Paleozoic Patagonian terrane has had more than sufficient time to conductively cool and stabilize. We suggest that this contrast in T_e between old (>1.5 Ga) and younger terranes probably reflects the larger thickness, depletion and, importantly, smaller water content of old (>~1.5 Ga) lithosphere, as has been suggested for Europe [*Pérez-Gussinyé and Watts*, 2005] and the western United States [*Lowry and Smith*, 1994].

[47] Within the Precambrian basement, there are four areas of relatively low T_e that coincide with sutures, rifts and sites of hot spot magmatism. Starting from the south, we encounter low T_e in the Paraná basin at ~27°S, located west of the region covered by flood basalts, where NW-SE oriented dyke swarms that fed the ~130 Myr Paraná flood basalts are exposed (Figure 6) [*Hawkesworth et al.*, 2000]. The large area of low T_e reaffirms the large scale of the feature evident in aeromagnetic surveys [*Milner et al.*, 1995]. Further west, this low T_e appears to propagate into the Chaco basin for the smallest window size used here, which also has the highest lateral resolution (Figure 6a).

[48] To the north, low T_e is observed along the SW-NE oriented Transbrasiliano suture from ~24° to ~14°S. This suture resulted from the collision of the Amazonian with the Sao Francisco and Rio de la Plata cratons during the Pan African orogeny [*Cordani and Sato*, 1999]. The southwestern part of this suture accommodated several igneous provinces consisting of alkaline intrusions at ~85–60 Ma. These have been related to the Trindade hot spot, currently located offshore Brazil in the Trindade islands [*Gibson et al.*, 1995, 1997].

[49] Along the eastern side of the Amazon basin, we estimate a low T_e region which, for the smallest window size used here, appears to continue westward into the Solimoes basin (Figure 6a). This low T_e may reflect Phanerozoic rifting that separated the Brazilian craton into the Guyana and Guaporé Shields.

[50] Finally, within the Guyana shield there is a linear SW-NE trending zone of low T_e along the Mesozoic Tacutu graben (Figure 6a). Coherence analysis centered in this area similarly finds low T_e [*Ojeda and Whitman*, 2002]. This graben likely formed along an older existing suture because it separates geological units of different Archean and Early/Middle Proterozoic age and nature [*Trompette*, 1994]. Moreover, this old suture may have been reactivated during the Late Triassic, providing the conduit through which flood basalts of the Central Atlantic Magmatic Province were emplaced at its northwestern end in Venezuela (Figure 6). Later tectonism along this suture occurred in Early Jurassic, when it functioned as a rift branch of the early stages of opening of the central Atlantic [*Sears et al.*, 2005]. In summary, within cratonic South America, low T_e often coincides with locations where tectonism has occurred repeatedly through geologic time.

5.2. *Te* and S-Wave Velocity

[51] Shear wave velocities are sensitive to rock temperature and composition, which also influence rheology and hence the integrated strength of the lithosphere. Consequently we expect a positive correlation between S velocity and T_e. Comparison of T_e and S velocity is not straightforward as, analogously to T_e estimates, shear wave velocity models depend on the methodology employed for their estimation and the data used for analysis. Moreover, the relative sensitivities of T_e and S velocity to temperature, mineral composition, fluids and partial melt are different. Nevertheless,

the latest models of S velocity for South America [*Heintz et al.*, 2005; *Feng et al.*, 2004; M. Feng et al., Upper mantle structure of South America from joint inversion of waveforms and fundamental-mode group velocities of Rayleigh waves, submitted to *Journal of Geophysical Research*, 2007 (hereinafter referred to as Feng et al., submitted manuscript, 2007)] compare favorably to our results. For visual comparison we show in Figure 6 the S-velocity model of Feng et al. (submitted manuscript, 2007) at 100 km depth. Their shear wave velocities are obtained from simultaneously inverting regional S and Rayleigh waveforms and fundamental-mode Rayleigh-wave group velocities (Feng et al., submitted manuscript, 2007).

[52] The resulting shear wave velocity and T_e maps correlate, in general, remarkably well. Common features found in the various tomographic models include high S velocity under the Guaporé, Guyana and Sao Francisco cratons and the Paraná and Parnaiba basins. All of these areas also exhibit high T_e (Figure 6). Note that T_e in excess of 70 km cannot be estimated with the window sizes used in our analysis, so we do not resolve differing T_e within regions of cratonic lithosphere. Hence, while S tomography indicates differing thicknesses for the cratonic Guaporé and Guyana shields, we depict these cratons as having apparently uniform high T_e (>70 km).

[53] On the other hand, low S velocity has been inferred under the southwestern end of the Transbrasiliano lineament (TBL) [*Feng et al.*, 2004; *Heintz et al.*, 2005; Feng et al., submitted manuscript, 2007] consistent with low P velocities in the SW and central segments of the TBL derived in local tomography with greater lateral resolution [*Schimmel et al.*, 2003; *Assumpçao et al.*, 2004]. The area of low P velocity along the TBL from the latter studies corresponds remarkably well with the low T_e estimated with the smallest window size (Figure 6a).

[54] Along the Amazonian-Solimoes basin, low S-velocities have been imaged by *Heintz et al.* [2005] but were not observed across the entire basin by *Feng et al.* [2004] and Feng et al. (submitted manuscript, 2007). Within the Amazon basin, Feng et al. (submitted manuscript, 2007) obtained lower S-wave velocities than in the surrounding shields (Figure 6f), which coincide with low T_e areas (Figures 6a and 6b), further supporting the view that the Amazon rifting system affected at least some parts of the lithosphere.

[55] Along the Andean plateau there is good correlation between slow seismic velocity and low T_e. The relationship is particularly notable where aseismic ridges subduct (Figures 6b and 6f). In areas where flat subduction occurs, i.e., southern Chile, northern Peru and perhaps northern Colombia, S velocity (Figure 6f) and T_e are, in general, relatively larger. For example, relatively greater T_e is clearly observed in northern Colombia with all three estimation windows (Figures 6a, 6b, and 6c). Greater T_e is also observed in northern Peru but is most clear with 600×600 km sampling (Figure 6b). Finally, greater T_e is observed in the flat slab area of Chile with 400×400 km sampling, but does not persist in larger windows. High S velocity of the lithospheric mantle above the Chilean flat slab has also been observed with local tomography [*Wagner et al.*, 2006], suggesting that corresponding high rigidity in Figure 6a is real. In subsequent work we discuss two possible reasons for the relationship between high S velocities and T_e at flat subduction zones (Pérez-Gussinyé et al., manuscript in preparation, 2007).

[56] Figure 8 summarizes the relationship between T_e and S velocities. Here we show a scatterplot of T_e estimates versus shear wave velocity at 100 km depth (red dots) sampled from the maps shown in Figure 6. Superimposed, we also show the mean value of T_e within 10 km bins versus the corresponding mean of S-velocity at 100 km (blue squares). Although the standard deviation of S-velocities in the relationship is large, T_e is positively correlated with S-velocity, as already suggested from visual comparison.

[57] There are numerous possible contributors to the scatter in the relationship. First and foremost, T_e and shear wave velocity are measuring two very different things. T_e is fundamentally an integral of the bending stress that supports lithospheric loads, and as such it is most sensitive to parameters of the power law creep rheology (i.e., temperature, mineral composition, water, and to a lesser degree strain rate) integrated over the entire crust and the uppermost mantle [e.g., *Lowry and Smith*, 1995]. Shear wave velocity is primarily a measure of rock shear rigidity (with a weak dependence on density) that is most sensitive to temperature, mineral composition, water and the presence of partial melt. The dependencies on temperature, mineral composition and water content have similar sign for both T_e and S velocity, which is responsible for the positive correlation between the two. However, the relative sensitivities to each of these fields are

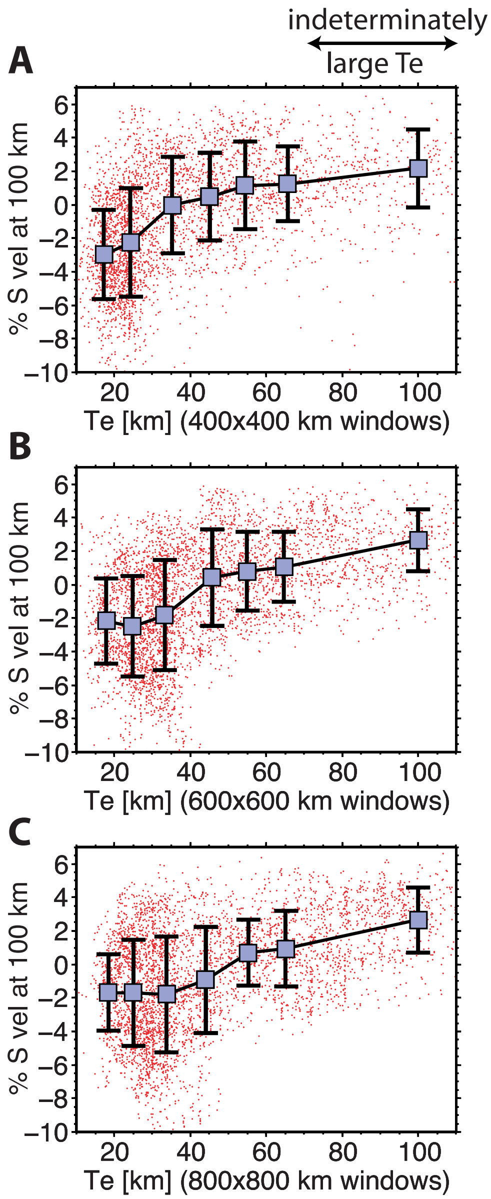

Figure 8. (a) Red dots are scatterplots of T_e estimates obtained using 400 × 400 km windows (Figure 6a) versus shear wave velocity at 100 km depth from Feng et al. (submitted manuscript, 2007) (Figure 6f). Blue squares represent the mean of T_e within 10 km bins versus mean S-velocities; bars are one standard deviation. (b and c) The same as in Figure 8a, but for T_e estimates obtained using 600 × 600 km and 800 × 800 km windows, respectively.

quite different. Considering these differences and the differences in depth-sampling (a complicated integral of properties in the crust and upper mantle versus a slice at 100 km depth) and in resolution of the measurements, the scatter in the relationship is not at all surprising.

[58] Effects of differences in spatial resolution are apparent in comparisons between T_e and S-velocities for different T_e estimation window sizes. T_e analyses for the 400 × 400 km windows yield far more estimates of less than 20 km than do the larger windows (compare, e.g., Figure 8a with Figures 8b and 8c). The smaller T_e estimates derived using larger windows are found predominantly in the Cordillera where both T_e and S velocity are most likely to be significantly perturbed by non-thermal effects. Simultaneously, smaller T_e that may be present in weak lineaments separating the cratons tends to be averaged out, resulting in a weaker correlation of T_e and S velocity for low T_e and larger windows. On the other hand, at the high end of the T_e range, the standard deviation of S-velocities is larger for estimates obtained with small windows than with larger ones (compare Figure 8a with Figure 8c). We believe that this results from the inability of small windows to recover large T_e (see Figures 4 and 5).

5.3. *Te* and Surface Heat Flow

[59] Heat flow data reflects the thermal state of the lithosphere and as such should also relate to T_e [*Lowry and Smith*, 1995]. However, uncertainties in the relationship of surface heat flow to temperature at depth can be large, as poorly known crustal heat production and dynamical effects of subduction, erosion, and hydrologic flow are all important contributors [e.g., *Mareschal and Jaupart*, 2004]. Also, heat flow measurements in South America are relatively sparse, and many measurements acquired by mining and oil companies are unreliable [*Hamza et al.*, 2005]. Thus any comparison of South American T_e and heat flow requires caution.

[60] We compare our T_e estimates to a recent compilation of heat flow in South America by *Hamza et al.* [2005]. Sampling locations are shown as black triangles in Figure 6e. *Hamza et al.* [2005] find generally lower heat flow (<60 mW/m^2) in the stable part of the continent than in the Andean cordillera (>70 mW/m^2). This first-order pattern of heat flow variation is in accord with our T_e estimates.

[61] Smaller scale variations in heat flow are also apparent in Figure 6e, which plots the measurements after subtracting a regional heat flow field. The regional heat flow is a polynomial representation of South American heat flow which is meant to represent the first-order westward increase from 60 mW/m^2 in the Stable Platform to 70 mW/m^2 in the Andes [*Hamza et al.*, 2005]. Within the stable

platform, higher than normal heat flow is observed near the southwestern part of the Transbrasiliano lineament and in the Amazon basin, both of which have lower T_e and shear wave velocities than the surrounding cratons (Figure 6) [*Feng et al.*, 2004; *Heintz et al.*, 2005; *Schimmel et al.*, 2003; Feng et al., submitted manuscript, 2007]. Correlation of high heat flow with low S velocity at 100 km depth suggests a correspondingly high geothermal gradient to lithospheric depths, resulting in the weak lithosphere observed in our T_e maps.

[62] Additionally, high heat flow is observed between the northern end of the Paraná basin and the southern end of the Sao Francisco craton (Figure 6e). However, this area does not exhibit low shear wave velocity or small T_e, suggesting that this heat flow anomaly reflects very shallow processes. Alternatively, this anomaly may have too small a lateral scale to be imaged by continent-scale studies of T_e and S velocity.

[63] Within the Andean cordillera, low heat flow is observed over the Chile, Peru and northern Colombia flat subduction zones. These areas are associated with relatively high S velocity and T_e, suggesting that here also low heat flow is representative of relatively low temperature at depth. In contrast, southern Chile (south of 30°S), the central Andes (between ~14° and 25°S) and Ecuador (~0°S) all have relatively high heat flow, low S velocity and low T_e (Figure 6). These are areas of normal-angle, as opposite to flat, subduction may thus have legitimately higher temperatures at shallow depth.

5.4. *Te* and Intracontinental Seismicity

[64] Intracontinental seismicity, far from plate boundaries, is thought to occur along zones such as failed rifts weakened by previous tectonic activity [e.g., *Sykes*, 1978], in areas where crustal inhomogeneities occur, for example large magmatic intrusions like those observed near the New Madrid seismic zone [*Campbell*, 1978], in areas of high heat flow, as also observed in the New Madrid seismic zone [*Liu and Zoback*, 1997], and where seismic velocities at depth are low [*Assumpçao et al.*, 2004].

[65] In Figure 6 we compare our T_e estimates to the intracontinental seismicity based on a catalogue of shallow (≤45 km) earthquakes in Brazil, Paraguay and Uruguay. The catalogue presented here is an updated version of that published by *Assumpçao et al.* [2004] (M. Assumpçao, personal communication, 2006). Because of the lack of seismic stations over part of the Brazilian territory this catalogue is only valid for the region east of 65°W and south of 6°N. The catalogue includes historical and instrumental data from 1861 to present and has been normalized to eliminate concentrations of events resulting from a greater population density or a larger distribution of seismic stations in particular areas (see *Assumpçao et al.* [2004] for a detailed explanation on the generation of the catalogue).

[66] *Assumpçao et al.* [2004] found a strong correlation between low seismic velocities and seismicity in southeastern Brazil, in an area located between 26° to 12°S and 58° to 43°W. Figure 6 suggests that the correlation between seismic velocities, seismicity and additionally low *Te* extends at broad-scale to the whole of Brazil, Paraguay and Uruguay. For example, seismicity concentrates west of the Paraná basin (in the area of the Asuncion dyke swarms, ~27°S), along the Transbrasiliano lineament, and along the Amazonian basin, where T_e and shear wave velocity are low. Interestingly, *Te* values along the Transbrasiliano lineament are low only in seismically active areas (Figure 6a). Because seismically active areas with low T_e are surrounded by rigid cratons, where seismicity is very sparse, we infer that the latter are strong enough to inhibit tectonism, leading to repeated focusing of deformation within the younger, weaker areas.

[67] The correlation between areas of low shear wave velocity, high heat flow and intracontinental seismicity probably implies that the topography of the lithosphere-asthenosphere boundary might play an important role in focusing seismicity within continental interiors, as proposed by *Assumpçao et al.* [2004] for southeast Brazil and *Liu and Zoback* [1997] for the New Madrid seismic zone in North America. These authors suggest that where the lithosphere is thinner than the surrounding areas, the geothermal gradient is higher, resulting in weakening of the mantle lithosphere and lower crust with respect to the surrounding regions. This leads to focusing of the far-field tectonic stress and concentration of seismicity within the brittle, upper part of the thinner lithosphere [*Assumpçao et al.*, 2004].

[68] We note that present-day seismic activity, as evidenced by intracontinental earthquakes, tends to focus in the same areas where past tectonic activity localized, e.g., west of the Parana flood basalts, along the Transbrasiliano lineament, the Amazonian basin and the Tacutu graben. Thus the differences in lithospheric flexural rigidity, thickness and geothermal gradients observed today between

these areas and the surrounding cratons are not transient, and must have been maintained, in some cases, for at least ~500 m.y. These differences in lithospheric structure probably reflect a higher mantle temperature and/or volatile content early in Earth's history, which lead, during the Archean and Early/Middle Proterozoic, to the formation of thicker and more depleted lithospheres which today are inherently more resistant to deformation than lithospheres formed subsequently, as has been inferred for Europe [*Pérez-Gussinyé and Watts*, 2005].

6. Conclusions

[69] We have estimated the *Te* structure of South America by modeling the coherence of continent-wide grids of topography and Bouguer gravity anomaly. The gravity anomaly was generated by combining sparsely distributed terrestrial measurements compiled by GETECH (UK) with a uniformly distributed data set from the EIGEN-CG30C model, which is a combination of terrestrial and free-air gravity derived from the satellites GRACE and CHAMP [*Foerste et al.*, 2005]. A spherical Bouguer correction was applied to the EIGEN-CG30C free-air gravity anomaly in order to preserve the true wavelength content in the Bouguer anomaly.

[70] Our results demonstrate a first-order pattern in which effective elastic thickness, T_e, of the stable South American platform is much higher than that of the Andean domain. T_e correlates remarkably well with other proxies for lithospheric structure. Areas of high T_e exhibit high seismic velocities at ~100 km depth and low surface heat flow. The excellent correlation of our results with shear wave velocity maps of the continent suggests that in the future, T_e maps may not only be used to better understand lithospheric mechanical properties, but also to image lateral variability of lithospheric structure (e.g., thickness and composition) analogously to how seismic velocities are currently used.

[71] We also find that within the stable South American platform, the Archean and Paleo/Middle-Proterozoic cratonic nuclei exhibit large T_e, as do the Parnaiba and Paraná basins which are thought to be underlain by old (~2 Ga) basement [*Cordani et al.*, 1984; *Brito Neves et al.*, 1984]. However, the Phanerozoic Patagonian terrane has generally lower T_e. Thus T_e is to first order dependent on terrane age. This dependence probably reflects the greater thickness and more depleted compositions of older terranes (>1.5 Ga old).

[72] Within the Precambrian basement of the stable platform, T_e variations are observed at regional scale: relatively lower T_e occurs at sites that have been repeatedly reactivated through geological history as major sutures, rift zones and sites of hot spot magmatism. Today, these low T_e areas concentrate most of the intracontinental seismicity and generally exhibit lower shear wave velocities and higher heat flow than the surrounding rigid cratons. It follows that cratonic interiors are strong enough to inhibit tectonism and that intracontinental deformation repeatedly focuses within thin, hot and hence weak lithosphere. Finally, the recurrence of the deformation throughout the Phanerozoic in the same low T_e areas probably implies that the differences in lithospheric flexural rigidity, thickness and geothermal gradients observed today between these areas and the surrounding cratons are not transient, and must have been maintained, in some cases, for at least ~500 m.y.

Acknowledgments

[73] We thank GETECH for providing the SAGAP gravity data used in this study. We thank M. Assumpçao and an anonymous reviewer for thoughtful reviews which helped improve this work. We also thank A. Tassara, Chris Swain, R. Hackney, J. Kirby, J. C. Mareschal, P. Audet, M. Schimmel, and M. Peres Rocha for many fruitful discussions on different issues presented in this paper. We also thank Chris Swain for providing the multitaper spectral estimation routines and some of the codes to generate synthetic data that were adapted for this investigation. A. Tassara provided the age data used in this study. We thank Mei Feng, M. Assumpçao, and V. Hamza for generously providing the shear wave velocity and heat flux data used in this study. M.P.G. thanks NERC, UK, and the Spanish Ministry of Science for financing this study.

References

Almeida, F. F. M., B. B. Brito Neves, and C. D. R. Carneiro (2000), The origin and evolution of the South American platform, *Earth Sci. Rev.*, *50*, 77–111.

Assumpçao, M., M. Schimmel, C. Escalante, J. R. Barbosa, M. Rocha, and L. V. Barros (2004), Intraplate seismicity in SE Brazil: Stress concentration in lithospheric thin spots, *Geophys. J. Int.*, *159*, 390–399, doi:10.1111/j.1365-246X.2004.02357.x.

Audet, P., and J.-C. Mareschal (2004), Variations in elastic thickness in the Canadian Shield, *Earth Planet. Sci. Lett.*, *226*, 17–31.

Banks, R. J., R. L. Parker, and S. P. Huestis (1977), Isostatic compensation on a continental scale: Local versus regional mechanisms, *Geophys. J. R. Astron. Soc.*, *51*, 431–452.

Basei, M. A. S., O. Siga Jr., H. Masquelin, O. M. Harara, J. M. Reis Neto, and F. P. Preciozzi (2000), The Dom Feliciano

Belt and the Rio de la Plata craton: Tectonic evolution and correlation with similar provinces of southwestern Africa, in *Tectonic Evolution of South America*, edited by U. G. Cordani et al., pp. 311–334, Tecton. Evol. of S. Am., Rio de Janeiro, Brazil.

Bassin, C., G. Laske, and G. Masters (2000), The current limits of resolution for surface wave tomography in North America, *Eos Trans. AGU*, *81*(48), Fall Meet Suppl., Abstract S12A-03.

Brito Neves, B. B., R. Fuck, U. G. Cordani, and A. Thomaz (1984), Influence of basement structures on the evolution of the major sedimentary basins of Brazil: A case of tectonic heritage, *J. Geodyn.*, *1*, 495–510.

Brito Neves, B. B., M. C. Campos Neto, and R. A. Fuck (1999), From Rodinia to western Gondwana: An approach to the Brasiliano–Pan African cycle and orogenic collage, *Episodes*, *22*, 155–166.

Brown, C. D., and R. J. Phillips (2000), Crust-mantle decoupling by flexure of continental lithosphere, *J. Geophys. Res.*, *105*, 13,221–13,238.

Burov, E., and M. Diament (1995), The effective elastic thickness (T_e) of the continental lithosphere: What does it really mean?, *J. Geophys. Res.*, *100*, 3905–3927.

Campbell, D. L. (1978), Investigation of the stress-concentration mechanism for intraplate earthquakes, *Geophys. Res. Lett.*, *5*, 477–479.

Cordani, U. G., and K. Sato (1999), Crustal structure of the South American Platform, based on Nd isotopic systematics from granitoid rocks, *Episodes*, *22*, 167–173.

Cordani, U. G., B. B. Brito Neves, R. A. Fuck, R. Porto, A. Thomaz Filho, and F. M. B. Cunha (1984), Estudo preliminar de integracao de pre-Cambriano com os eventos tectonicos das bacias sedimentares Brasileiras, *Bul. Cienc. Tec. Pet. Secao*, *15*, 70 pp.

Dorbath, C., M. Granet, G. Poupinet, and C. Martinez (1993), A teleseismic study of the Altiplano and the eastern Cordillera in northern Bolivia: New constraints on a lithospheric model, *J. Geophys. Res.*, *98*, 9825–9844.

Feng, M., M. Assumpcao, and S. Van der Lee (2004), Group velocity tomography and lithospheric *S*-velocity structure of the South American continent, *Phys. Earth Planet. Inter.*, *147*, 315–331.

Foerste, C., et al. (2005), A new high resolution global gravity field model derived from combination of GRACE satellite mission and altimetry/gravimetry surface gravity data, *Geophys. Res. Abstr.*, *7*, 04561.

Forsyth, D. W. (1985), Subsurface loading estimates of the flexural rigidity of continental lithosphere, *J. Geophys. Res.*, *90*, 12,623–12,632.

Gibson, S. A., R. N. Thompson, O. H. Leonardos, A. P. Dickin, and J. G. Mitchell (1995), The Late Cretaceous impact of the Trindade mantle plume: Evidence from large-volume, mafic potassic magamatism in SE Brazil, *J. Petrol.*, *36*, 189–228.

Gibson, S. A., R. N. Thompson, R. K. Weska, A. P. Dickin, and O. H. Leonardos (1997), Late Cretaceous rift-related upwelling and melting of the Trindade starting mantle plume head beneath western Brazil, *Contrib. Mineral. Petrol.*, *126*, 303–314.

Green, C. M., and J. D. Fairhead (1991), The South American Gravity Project, in *Recent Geodetic and Gravimetric Research in Latin America*, edited by W. Torge, A. Fletcher, and J. Tanner, pp. 82–95, Springer, New York.

Hamza, V., F. J. S. Silva Dias, A. J. L. Gomes, and Z. G. Delgadilho Terceros (2005), Numerical and functional representations of regional heat flow in South America, *Phys. Earth Planet. Inter.*, *152*, 223–256.

Hawkesworth, C. J., K. Gallagher, L. Kirstein, M. S. M. Mantovani, D. W. Peate, and S. P. Turner (2000), Tectonic controls on magamatism associated with continental breakup: An example from the Paraná-Entdeka Province, *Earth Planet. Sci. Lett.*, *179*, 335–349.

Heintz, M., E. Debayle, and A. Vauchez (2005), Upper mantle structure of the South American continent and neighboring oceans from surface wave tomography, *Tectonophysics*, *406*, 115–139.

Hirth, G., and D. L. Kohlstedt (1996), Water in oceanic upper mantle: Implications for rheology, melt extraction and the evolution of the lithosphere, *Earth Planet. Sci. Lett.*, *144*, 93–108.

Jordan, T. H. (1978), Composition and development of the continental lithosphere, *Nature*, *274*, 544–548.

Kirby, J. F. (2005), Which wavelet best reproduces the Fourier power spectrum?, *Comput. Geosci.*, *31*, 846–864.

Kirby, J. F., and C. J. Swain (2004), Global and local isostatic coherence from the wavelet transform, *Geophys. Res. Lett.*, *31*, L24608, doi:10.1029/2004GL021569.

Latychev, K., J. X. Mitrovica, M. E. Tamisiea, J. Tromp, and R. Moucha (2005), Influence of lithospheric thickness variations on 3-D crustal velocities due to glacial isostatic adjustment, *Geophys. Res. Lett.*, *32*, L01304, doi:10.1029/2004GL021454.

Liu, L., and M. D. Zoback (1997), Lithospheric strength and intraplate seismicity in the New Madrid seismic zone, *Tectonics*, *16*, 585–595.

Lowry, A. R., and R. B. Smith (1994), Flexural rigidity of the Basin and Range–Colorado Plateau–Rocky Mountain transition from coherence analysis of gravity and topography, *J. Geophys. Res.*, *99*, 20,123–20,140.

Lowry, A. R., and R. B. Smith (1995), Strength and rheology of the western US Cordillera, *J. Geophys. Res.*, *100*, 17,947–17,963.

Lowry, A. R., and S. Zhong (2003), Surface versus internal loading of the Tharsis rise, Mars, *J. Geophys. Res.*, *108*(E9), 5099, doi:10.1029/2003JE002111.

Lowry, A. R., N. M. Ribe, and R. B. Smith (2000), Dynamic elevation of the Cordillera, western United States, *J. Geophys. Res.*, *105*, 23,371–23,390.

Macario, A., A. Malinverno, and W. F. Haxby (1995), On the robustness of elastic thickness estimates, and the strength of the continental lithosphere, *J. Geophys. Res.*, *100*, 15,163–15,172.

Mandelbrot, B. B. (1983), *The Fractal Geometry of Nature*, W.H. Freeman, New York.

Mantovani, M. S. M., S. R. C. de Freitas, and W. Shukowsky (2001), Tidal gravity anomalies as a tool to measure rheological properties of the continental lithosphere: Application to the South American Plate, *J. S. Am. Sci.*, *14*, 2–14.

Mantovani, M. S. M., W. Shukowsky, S. R. C. de Freitas, and B. B. Brito Neves (2005a), Lithosphere mechanical behaviour inferred from tidal gravity anomalies: A comparison of Africa and South America, *Earth Planet. Sci. Lett.*, *230*, 397–412.

Mantovani, M. S. M., M. C. L. Quintas, W. Shukowsky, and B. B. Brito Neves (2005b), Delimitation of the Paranapanema Proterozoic block: A geophysical contribution, *Episodes*, *28*, 18–22.

Mareschal, J. C., and C. Jaupart (2004), Variations of surface heat flow and lithospheric thermal structure beneath the North American craton, *Earth Planet. Sci. Lett.*, *223*, 65–77.

McKenzie, D. (2003), Estimating T_e in the presence of internal loads, *J. Geophys. Res.*, *108*(B9), 2438, doi:10.1029/2002JB001766.

Milner, S. C., A. R. Duncan, A. M. Whittingon, and A. Ewart (1995), Trans-Atlantic correlation of eruptive sequences and individual silicic volcanic units within the Paraná-Etendeka province, *J. Volcanol. Geotherm. Res.*, *69*, 137–157.

Ojeda, G. Y., and D. Whitman (2002), Effect of windowing on lithosphere elastic thickness estimates obtained via the coherence method: Results from northern South America, *J. Geophys. Res.*, *107*(B11), 2275, doi:10.1029/2000JB000114.

O'Reilly, S. Y., W. L. Griffin, Y. H. Poudjom Djomani, and P. Morgan (2001), Are lithospheres forever? Tracking changes in the subcontinental mantle through time, *GSA Today*, *11*, 4–10.

Parker, R. L. (1972), The rapid calculation of potential anomalies, *Geophys. J. R. Astron.*, *31*, 447–455.

Percival, D. B., and A. T. Walden (1993), *Spectral Analysis for Physical Applications, Multitaper and Conventional Univariate Techniques*, pp. 1–190, Cambridge Univ. Press, New York.

Pérez-Gussinyé, M., and A. B. Watts (2005), The long-term strength of Europe and its implications for plate forming processes, *Nature*, *436*, 381–384, doi:10.1038/nature03854.

Pérez-Gussinyé, M., A. R. Lowry, A. B. Watts, and I. Velicogna (2004), On the recovery of effective elastic thickness using spectral methods: Examples from synthetic data and from the Fennoscandian Shield, *J. Geophys. Res.*, *109*, B10409, doi:10.1029/2003JB002788.

Pérez-Gussinyé, M., A. R. Lowry, A. B. Watts, and J. Phipps Morgan (2006), Tracing lithospheric structure using flexural rigidity in South America: Implications for intra-continental deformation and subduction geometry, *Eos Trans. AGU*, *87*(52), Fall Meet. Suppl., Abstract T51A-1518.

Phipps Morgan, J., T. J. Reston, and C. R. Ranero (2004), Contemporaneous mass extinctions flood basalts and 'impact signals': Are mantle plume-induced lithospheric gas explosions the causal link?, *Earth Planet. Sci. Lett.*, *217*, 263–284.

Polet, J., P. Silver, G. Zandt, S. Ruppert, G. Bock, R. Kind, A. Reudoff, G. Asch, S. Beck, and T. Wallace (2000), Shear wave anisotropy beneath the Andes from the BANJO, SEDA, and PISCO experiments, *J. Geophys. Res.*, *105*, 6287–6304.

Pollack, H. N. (1986), Cratonization and thermal evolution of the mantle, *Earth Planet. Sci. Lett.*, *80*, 175–182.

Ramos, V. A. (2000), The southern Central Andes, in *Tectonic Evolution of South America*, edited by U. G. Cordani, A. Thomaz Filho, and D. A. Campos, pp. 561–604, Tecton. Evol. of S. Am., Rio de Janeiro, Brazil.

Schimmel, M., M. Assumpção, and J. C. VanDecar (2003), Seismic velocity anomalies beneath SE Brazil from *P* and *S* wave travel time inversions, *J. Geophys. Res.*, *108*(B4), 2191, doi:10.1029/2001JB000187.

Schobbenhaus, C., and A. Bellizia (2001), Geological map of South America, scale 1:5000000, Geol. Surv. of Braz., Brasilia.

Sears, J. W., G. M. St. George, and J. C. Winne (2005), Continental rift systems and anorogenic magmatism, *Lithos*, *80*, 147–154.

Simons, F. J., M. T. Zuber, and J. Korenaga (2000), Spatiospectral localization of isostatic coherence anisotropy in Australia and its relation to seismic anisotropy: Implications for lithospheric deformation, *J. Geophys. Res.*, *105*, 19,163–19,184.

Slepian, D. (1978), Prolate spheroidal wave functions, Fourier analysis and uncertainty, V, The discrete case, *Bell Syst. Tech. J.*, *57*, 1031–1042.

Snoke, J. A., and D. E. James (1997), Lithospheric structure of the Chaco and Paraná basins of South America from surface-wave inversion, *J. Geophys. Res.*, *102*, 2939–2951.

Stewart, J. (1998), Gravity anomalies and lithospheric flexure: Implications for the thermal and mechanical evolution of the continental lithosphere, Ph.D. thesis, Oxford Univ., Oxford, U. K.

Stewart, J., and A. B. Watts (1997), Gravity anomalies and spatial variations of flexural rigidity at mountain ranges, *J. Geophys. Res.*, *102*, 5327–5352.

Swain, C. J., and J. F. Kirby (2003), The effect of "noise" on estimates of effective elastic thickness of the continental lithosphere by the coherence method, *Geophys. Res. Lett.*, *30*(11), 1574, doi:10.1029/2003GL017070.

Swain, C. J., and J. F. Kirby (2006), An effective elastic thickness map of Australia from wavelet transforms of gravity and topography using Forsyth's method, *Geophys. Res. Lett.*, *33*, L02314, doi:10.1029/2005GL025090.

Sykes, L. R. (1978), Intraplate seismicity, reactivation of preexisting zones of weakness, alkaline magmatism, and other tectonism postdating continental fragmentation, *Rev. Geophys.*, *16*, 621–688.

Syracuse, E. M., and G. A. Abers (2006), Global compilation of variations in slab depth beneath arc volcanoes and implications, *Geochem. Geophys. Geosyst.*, *7*, Q05017, doi:10.1029/2005GC001045.

Tassara, A. (2005), Interaction between the Nazca and South American plates and formation of the Altiplano-Puna plateau: Review of a flexural analysis along the Andean margin (15°–34°S), *Tectonophysics*, *399*, 39–57.

Tassara, A., C. Swain, R. Hackney, and J. Kirby (2007), Elastic thickness structure of South America estimated using wavelets and satellite-derived gravity data, *Earth Planet. Sci. Lett.*, *253*, 17–36.

Thompson, D. J. (1982), Spectrum estimation and harmonic analysis, *Proc. IEEE*, *70*, 1055–1096.

Trompette, R. (1994), *Geology of Western Gondwana (2000–500 Ma)*, 341 pp., A. A. Balkema, Brookfield, Vt.

Turcotte, D. (1997), *Fractals and Chaos in Geology and Geophysics*, Cambridge Univ. Press, New York.

Turner, S., M. Regelous, S. Kelley, and S. Hawkesworth (1994), Magmatism and continental break-up in the South Atlantic: High precision ^{40}Ar-^{39}Ar geochronology, *Earth Planet Sci. Lett.*, *121*, 333–348.

Vidotti, R. M. (1997), Lithospheric structure beneath the Paraná and Parnaiba basins, Brazil, from regional gravity analyses, Ph.D. thesis, School of Earth Sci., Univ. of Leeds, Leeds, U. K.

Vidotti, R. M., C. J. Ebinger, and J. D. Fairhead (1998), Gravity signature of the western Paraná basin, Brazil, *Earth Planet. Sci. Lett.*, *159*, 117–132.

Wagner, L. S., S. Beck, G. Zandt, and M. N. Ducea (2006), Depleted lithosphere, cold, trapped, and frozen melt puddles above the flat slab in central Chile and Argentina, *Earth Planet. Sci. Lett.*, *245*, 289–301.

Watts, A. B. (2001), *Isostasy and Flexure of the Lithosphere*, Cambridge Univ. Press, New York.

Watts, A. B., J. H. Bodine, and M. S. Steckler (1980), Observations of the flexure and the state of stress in the oceanic lithosphere, *J. Geophys. Res.*, *85*, 6369–6376.

Watts, A. B., S. H. Lamb, J. D. Fairhead, and J. F. Dewey (1995), Lithospheric flexure and bending of the Central Andes, *Earth Planet. Sci Lett.*, *134*, 9–21.

Wieczorek, M. A., and R. J. Phillips (1998), Potential anomalies on a sphere: Applications to the thickness of the lunar crust, *J. Geophys. Res.*, *103*, 1715–1724.

Willett, S. D., D. S. Chapman, and H. J. Neugebauer (1984), Mechanical response of the continental lithosphere to loading: Effect of thermal regimes, *Ann. Geophys.*, *2*, 679–688.

Willett, S. D., D. S. Chapman, and H. J. Neugebauer (1985), A thermo-mechanical model of continental lithosphere, *Nature*, *314*, 520–523.

Wyer, P. (2003), Statistical studies of seafloor geomorphology, Ph.D. thesis, Oxford Univ., Oxford, U. K.